



# CHORUS

This is the accepted manuscript made available via CHORUS. The article has been published as:

## Single particle configurations in $^{61}\text{Ni}$

S. Samanta, S. Das, R. Bhattacharjee, S. Chatterjee, R. Raut, S. S. Ghugre, A. K. Sinha, U. Garg, Neelam, N. Kumar, P. Jones, Md. S. R. Laskar, F. S. Babra, S. Biswas, S. Saha, P. Singh, and R. Palit

Phys. Rev. C **99**, 014315 — Published 24 January 2019

DOI: [10.1103/PhysRevC.99.014315](https://doi.org/10.1103/PhysRevC.99.014315)

# Single Particle Configurations in $^{61}\text{Ni}$

S. Samanta, S. Das, R. Bhattacharjee, S. Chatterjee, R. Raut,\* and S. S. Ghugre  
*UGC-DAE Consortium for Scientific Research, Kolkata Centre, Kolkata 700098, India*

A. K. Sinha

*UGC-DAE Consortium for Scientific Research, University Campus, Khandwa Road, Indore 452017, India*

U. Garg

*Department of Physics, University of Notre Dame, Notre Dame, Indiana 46556*

Neelam

*Department of Physics and Astrophysics, University of Delhi, New Delhi 110007, India*

N. Kumar

*Government Degree College, Dhaliara, District Kangra, Himachal Pradesh 177103, India*

P. Jones

*Department of Subatomic Physics, iThemba LABS, Somerset West 7129, South Africa*

Md. S. R. Laskar, F. S. Babra, S. Biswas, S. Saha, P. Singh, and R. Palit  
*Tata Institute of Fundamental Research, Mumbai 400005, India*

(Dated: January 1, 2019)

Excited states of the  $^{61}\text{Ni}$  ( $Z = 28, N = 33$ ) nucleus have been probed using heavy-ion induced fusion evaporation reaction and an array of Compton suppressed germanium (clover) detectors as detection system for the emitted  $\gamma$  rays. Seventeen new transitions have been identified and placement of six transitions have been modified with respect to the previous measurements, following which the level scheme of the nucleus has been extended upto an excitation energy  $E_x \sim 7$  MeV and spin  $\sim 10\hbar$ . Higher excitations involving the  $g_{9/2}$  orbital in the  $fpg$  model space have been established. The experimental results on the level structure of the nucleus have been interpreted in the light of large basis shell model calculations that lead to an understanding of the single particle configurations underlying the level structure of the nucleus. The comparison can be suggestive of further refinements in the shell model interactions for better overlap of the theoretical results with the experimental data.

PACS numbers: 23.20.Lv, 21.10.Hw, 21.60.Cs

## I. INTRODUCTION

Nuclei in the vicinity of the doubly-magic  $^{56}\text{Ni}$ -core ( $Z = 28, N = 28$ ) have been probed in a number of spectroscopic endeavors over the last couple of decades. The impetus of such studies has been manifold. At lower excitations, the level structure of these isotopes can be interpreted through particle excitations in the model space spanned by  $1f_{5/2}$ ,  $2p_{3/2}$ ,  $2p_{1/2}$  and  $1g_{9/2}$  orbitals [1]. This caters to the possibility of implementing shell model calculations and test the associated Hamiltonians and interactions in the process. The evolving structural features in these nuclei, with increasing excitation energy and spin, have also been of interest. At higher excitations, the same nuclei have been known to exhibit collectivity, magnetic rotation (MR) bands and core-broken configurations [2]. Thus,

investigating the excitation scheme of nuclei in the proximity of the  $^{56}\text{Ni}$ -core, especially using the contemporary spectroscopic tools, can be edifying in the light of the varied structural phenomena possible therein.

The  $^{61}\text{Ni}$  ( $Z = 28, N = 33$ ) nucleus with 5 neutrons outside the  $^{56}\text{Ni}$  core represents a prospective case in the aforementioned context. The nucleus has been previously studied by Wadsworth *et al.* [3, 4], following its population in  $\alpha$  and heavy-ion induced reaction, albeit using modest detection setups consisting of, atmost, few Ge(Li) detectors. The level scheme of the nucleus was extended to an excitation energy of  $\sim 5$  MeV along with limited or tentative spin-parity assignments. Subsequent work on the same nucleus by Warburton *et al.* [5] using heavy-ion induced fusion-evaporation reaction and Ge(Li) detectors largely confirmed the findings of Wadsworth *et al.* but reported only limited new level structure information. The nucleus was experimentally investigated also by Meyer *et al.* [6] following its population in the excited states from the decay of  $^{61}\text{Cu}$

---

\*Electronic address: rraut@alpha.iuc.res.in

( $Z = 29, N = 32$ ) and the resulting excitation scheme was largely similar to that proposed by Wadsworth *et al.*. Many of these experimental studies referred to the shell model calculations by Koops and Glaudemans [7], extensively carried out for nuclei around the  $^{56}\text{Ni}$ -core, in order to interpret the observed level scheme. The negative parity states at lower excitation energies, in  $^{61}\text{Ni}$ , were represented through single particle configurations in the model space consisting of  $2p_{3/2}$ ,  $1f_{5/2}$ , and  $2p_{1/2}$  orbitals, using the Modified Surface Delta Interaction (MSDI) and the Adjusted Surface Delta Interaction (ASDI), wherefrom it was noted that the level spacings were better reproduced with the latter. Wadsworth *et al.* [3] had also reported observation of positive parity states in the  $^{61}\text{Ni}$  nucleus at higher excitations that were perceived as coupling of the  $1g_{9/2}$  particle to the  $^{60}\text{Ni}$ -core. Shell model calculations including the  $1g_{9/2}$  orbital, for reproducing the positive parity states, were outside the purview of the aforesaid theoretical efforts presumably owing to the dimensional limitations of the erstwhile computational resources. Earlier studies on the nucleus also include that by Satyanarayana *et al.* [8] who studied the offline decay of  $^{61}\text{Cu}$ , produced in  $\alpha$ -induced in-beam reaction, to investigate the level structure of  $^{61}\text{Ni}$ . Still recently, Raman *et al.* studied [9] the thermal neutron capture on  $^{58-60}\text{Ni}$  isotopes and, in the process, reported a list of  $\gamma$ -ray transitions along with the de-exciting levels in the product nuclei, including  $^{61}\text{Ni}$ . It was a singles measurement, carried out with one Compton suppressed HPGe detector positioned at a fixed geometry, and obviously had no scope for determining the coincidence relationships between the observed transitions or identifying their multipole and electromagnetic character or making spin-parity assignments to the excited levels.

A detailed study of the level structure of the  $^{61}\text{Ni}$  nucleus both experimentally, using the contemporary high resolution and efficient spectroscopic tools, and theoretically, using the updated theoretical models, is thus warranted and such an endeavor is reported in this paper.

## II. EXPERIMENTAL DETAILS AND DATA ANALYSIS

Excited states of the  $^{61}\text{Ni}$  nucleus were populated using the  $^{59}\text{Co}(^7\text{Li},\alpha n)$  reaction at  $E_{lab} = 22-24$  MeV. The  $^7\text{Li}$  beam was obtained from the Pelletron LINAC Facility at the Tata Institute of Fundamental Research (TIFR), Mumbai. The target was  $5.2$  mg/cm $^2$  of mono-isotopic  $^{59}\text{Co}$  evaporated on a  $4$  mg/cm $^2$  thick Ta-foil, fabricated at the TIFR Target Laboratory. The  $\gamma$  rays emitted from the de-exciting nuclei were detected using an array of 11 Compton suppressed germanium (clover) detectors positioned at  $90^\circ$  (4 detectors),  $115^\circ$  (1 detector),  $140^\circ$  (3 detectors) and  $157^\circ$  (3 detectors). The pulse processing and data acquisition system was one

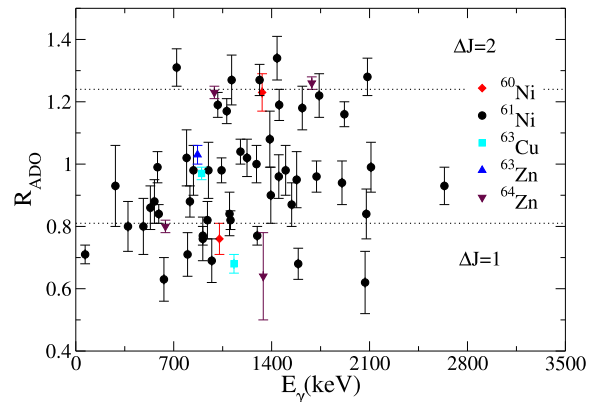


FIG. 1: (Color Online)  $R_{ADO}$  values for different transitions of  $^{61}\text{Ni}$  along with those of selected transitions of previously known multiplicities from other nuclei populated in the present experiment. The latter is used to fix the reference values used in the current analysis as well as for validation of the same.

based on Pixie-16 100 MHz 12-bit digitizers from XIA LLC, USA [10]. In-beam listmode data was acquired under the trigger condition of at least two Compton suppressed clovers firing in coincidence and  $\sim 1 \times 10^9$  events of multiplicity  $\geq 2$  were recorded during the experiment.

The acquired data was sorted into symmetric and angle-dependent  $\gamma$ - $\gamma$  matrices as well as  $\gamma$ - $\gamma$ - $\gamma$  cube for determining the coincidence relations between the observed  $\gamma$  rays along with their angular correlation and linear polarization. These informations are used to identify the placement of the transitions in the level scheme and establish their multipolarity and electromagnetic character so as to deduce the excitation pattern of the nuclei of interest and understand the underlying physics therefrom. The energy calibration was carried out using standard radioactive sources of  $^{152}\text{Eu}$  and  $^{133}\text{Ba}$ . The calibration at higher energies ( $\gtrsim 2$  MeV) was verified using the  $\gamma$  rays from in-beam products, known from earlier measurements. The reduction of the listmode data into matrices and cube was carried out using the MARCOS code [10] and the RADWARE [11] package was used for the subsequent analysis.

The multiplicities of the  $\gamma$ -ray transitions were assigned from their Ratio of Angular Distribution from Oriented nuclei ( $R_{ADO}$ ) [12], defined as,

$$R_{ADO} = \frac{I_{\gamma_1} \text{ at } 140^\circ \text{ (Gated by } \gamma_2 \text{ at all angles)}}{I_{\gamma_1} \text{ at } 115^\circ \text{ (Gated by } \gamma_2 \text{ at all angles)}} \quad (1)$$

where  $I_{\gamma_1}$  indicates the intensity of the  $\gamma$ -ray transition of interest. In the present setup, the  $R_{ADO}$  value for

pure quadrupole transitions is  $1.24 \pm 0.02$  and for pure dipole transitions is  $0.81 \pm 0.01$ . A  $R_{ADO}$  value between those for pure transitions, 0.81 and 1.24, would indicate mixed multipolarity with the mixing ratio  $\delta > 0$ , while a value less than 0.81 would imply a negative mixing ratio. Fig. 1 illustrates the plot of  $R_{ADO}$  values of  $\gamma$ -ray transitions from  $^{61}\text{Ni}$  along with those used to determine the reference values. Further details of this analysis procedure can be found in Ref.[1].

For possible  $\gamma$ -ray transitions, the multipolarities were also assigned from the Ratio of Directional Correlation from Oriented ( $R_{DCO}$ ) nuclei that is defined as,

$$R_{DCO} = \frac{I_{\gamma_1} \text{ at } 140^\circ \text{ (Gated by } \gamma_2 \text{ at } 90^\circ)}{I_{\gamma_1} \text{ at } 90^\circ \text{ (Gated by } \gamma_2 \text{ at } 140^\circ)} \quad (2)$$

where  $I_{\gamma_1}$  implies the same as in Eq. (1). In the present detector geometry,  $R_{DCO}$  of a pure quadrupole transition is  $0.95 \pm 0.01$  in pure quadrupole gate and  $1.74 \pm 0.01$  in pure dipole gate. The same values for pure dipole are  $0.59 \pm 0.01$  and  $0.96 \pm 0.02$ , respectively.

The use of clover detectors in the present work facilitated the determination of linear polarization of the observed  $\gamma$ -ray transitions, albeit with considerable uncertainties owing to the limited number of detectors at  $90^\circ$  that are used for the purpose. The polarization value is indicative of the electromagnetic (electric or magnetic) character of the  $\gamma$ -ray transition and is determined from the asymmetry ( $\Delta$ ) between its scattering in the perpendicular and the parallel planes with respect to the reaction plane. The asymmetry is quantitatively defined as,

$$\Delta = \frac{aN_{\perp} - N_{\parallel}}{aN_{\perp} + N_{\parallel}} \quad (3)$$

where  $N_{\perp}$  and  $N_{\parallel}$  are the number of scattered photons, of a given  $\gamma$  ray, perpendicular and parallel to the reference plane, respectively. The term  $a$  is the geometrical asymmetry inherent in the detection setup defined by,  $a = N_{\parallel}/N_{\perp}$ , with respect to the scattering of  $\gamma$  rays from an unpolarized radioactive source. This was determined to be  $1.017 \pm 0.004$  (Fig. 2a). Details of the analysis procedure can be found in Ref. [1]. Fig. 2b depicts the  $\Delta$  values for the  $\gamma$ -ray transitions of  $^{61}\text{Ni}$  along with some of those with previously known electromagnetic nature, included as validation of the current analysis. A positive value of  $\Delta$  is indicative of an electric nature of the transition while a negative value implies that the  $\gamma$ -ray transition is magnetic. A near-zero  $\Delta$  usually signifies a mixed electromagnetic character. However, it may be noted that the value of  $\Delta$  extracted from the difference in the (Compton) scattering in perpendicular and parallel directions, is dependent on the energy of the incident  $\gamma$  ray. This

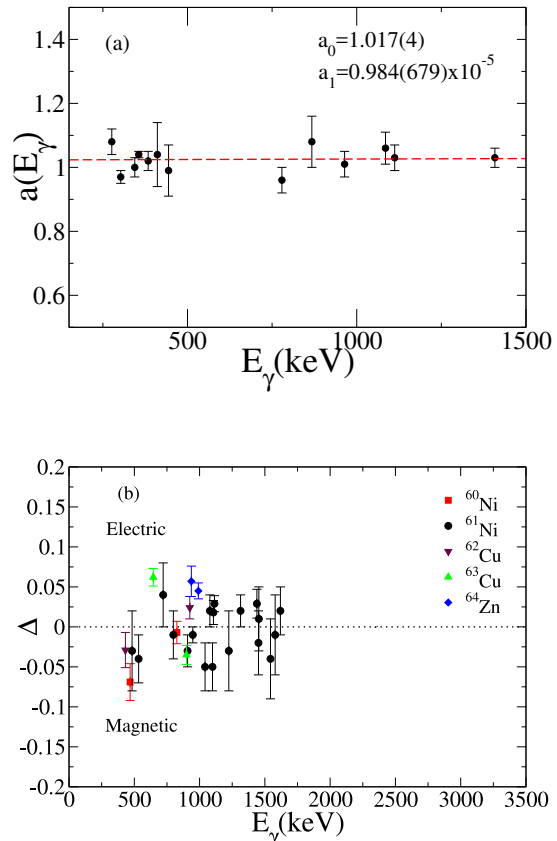


FIG. 2: (Color Online) (Upper Panel) Plot of the geometrical asymmetry ( $a$ ) against  $\gamma$ -ray energies along with the fit to the data points using the equation  $a_0 + a_1 * E_{\gamma}$ . (Lower Panel) Plot of polarization asymmetry  $\Delta$  (defined in Eq. 3) for different  $\gamma$ -ray transitions of the  $^{61}\text{Ni}$  nucleus along with those from other nuclei produced in the same experiment.

dependence can be accounted for by normalizing the asymmetry with what is called the polarization sensitivity ( $Q$ ) and considering the polarization ( $P$ ) value of a  $\gamma$ -ray transition, that were extracted using the procedure described in Ref.[1, 13] and is illustrated in Fig. 3.

The level structure of the  $^{61}\text{Ni}$  nucleus was constructed from the coincidence relationships between the observed  $\gamma$ -ray transitions, their intensities, multipolarities (from the  $R_{ADO}$  and  $R_{DCO}$  measurements) and their electromagnetic nature (indicated by the linear polarization). The experimental results were compared with the theoretical calculations for interpreting the excitation mechanisms associated with the level structure of the nucleus. The results of the exercise are presented and discussed in the next section.

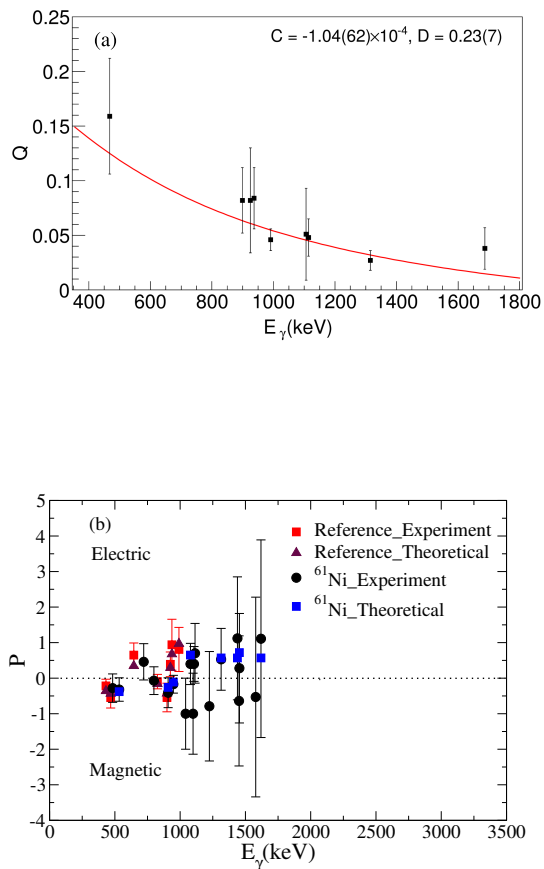


FIG. 3: (Color Online)(Upper Panel) Plot of polarization sensitivity as a function of  $\gamma$ -ray energy, determined from the observed  $\gamma$  rays of previously known multipole mixing ratio, along with the fit using the equation  $Q(E_\gamma) = Q_0(E_\gamma)(CE_\gamma + D)$  ( $Q_0(E_\gamma) = \frac{\alpha+1}{\alpha^2+\alpha+1}$ ,  $\alpha = E_\gamma/m_e c^2$ ,  $m_e c^2$  being electron rest mass energy). (Lower Panel) Plot of polarization  $P$ , defined by  $P = \Delta/Q$ , for different  $\gamma$ -ray transitions of  $^{61}\text{Ni}$  and other nuclei populated in the present experiment. The latter are of previously known multipole mixing that was used to calculate their theoretical polarization, included in the plot, for reference and validation of the current analysis.

### III. RESULTS AND DISCUSSIONS

The level scheme of the  $^{61}\text{Ni}$  nucleus, resulting from the present measurements, is illustrated in Fig. 4. Seventeen new  $\gamma$ -ray transitions have been assigned in the excitation pattern herein. In addition, there are six transitions, previously identified by Raman *et al.* [9], that were either differently placed or unplaced in the level scheme and the same has been reassigned following the current investigation. The 1590 keV transition, identified to be de-exciting the 3710 keV ( $J^\pi = 11/2^+$ ) level in this study, might be the 1588 keV transition from a 3711 keV level proposed by Raman *et al.* [9]. Nevertheless, this has been listed as a new transition in this work owing to the more complete (multipolarity and spin-parity) information obtained

herefrom. Wadsworth *et al.* [3] had identified a 1523-keV transition de-exciting a 3644-keV level but the same could not be confirmed in the present study. Similarly, the 1297-keV transition placed by Wadsworth *et al.* [3], to be de-exciting the 5316-keV state, has actually been established as a 1292-keV  $\gamma$  ray, de-populating a 5310-keV level, in the present study and has been listed as a new transition observed herein. It may be noted that the present experimental setup with an array of Compton suppressed germanium (clover) detectors is presumably more efficient than the setups used in the aforementioned (previous) studies and is facilitated with better statistics. The level structure of the nucleus has been extended upto an energy of  $\sim 7$  MeV and a spin  $\sim 10\hbar$ . The excitation pattern is typical of near spherical nuclei in the proximity of shell closures and exhibits the characteristic complexity. Representative  $\gamma$ -ray gated spectra, extracted from  $\gamma$ - $\gamma$  matrix and indicating the coincidence relations between the observed transitions, are illustrated in Fig. 5. An interesting feature of the present level scheme is a group of high energy  $\gamma$ -ray transitions, with  $E_\gamma \sim 2.5$ -3.0 MeV, de-exciting high spin even parity states. The observation of these transitions actually speak favorably of the detection system used in the current study. One such transition is the 2871-keV, de-populating the 4999-keV level, and the gated spectrum on this ( $\gamma$  ray) has been illustrated in Fig. 5(c) showing previously known transitions of  $^{61}\text{Ni}$ . As elaborated in the subsequent text, these high energy transitions can be attributed to de-excitation from the  $1g_{9/2}$  orbital to the  $fp$  orbitals. Fig. 6 depicts a spectrum generated with a sum of  $\gamma$ - $\gamma$  gates applied on the  $\gamma$ - $\gamma$ - $\gamma$  cube, that further aided in identifying the coincidences and facilitated the construction of the level scheme. The spin-parity assignments therein have been made from the  $R_{DCO}$ ,  $R_{ADO}$  and linear polarization measurement of the observed  $\gamma$ -ray transitions as well as comparison with the shell model calculations. Table 1 summarizes the level and  $\gamma$ -ray transition properties of the  $^{61}\text{Ni}$  nucleus, as derived from the current measurements and, for specific cases, adopted from the existing literature.

The principal output of the present experimental investigation pertains to the observation of higher excited states in the  $^{61}\text{Ni}$  nucleus, beyond the existing level scheme, and transitions therefrom. In the light of the previous shell model calculations in this nucleus, it is logical to attempt interpreting these states in terms of particle excitations to higher lying orbitals, say  $1g_{9/2}$ , and even look for signatures of core breaking. Large basis shell model calculations have been carried out using the NuShellX@MSU [14, 15] code running on a High Performance Computing (HPC) facility at UGC-DAE CSR, Kolkata Centre. The  $fp$  model space was chosen for the purpose and consisted of  $1f_{5/2}$ ,  $2p_{3/2}$ ,  $2p_{1/2}$  and  $1g_{9/2}$  orbitals. The calculations were unrestricted, meaning that the 5 neutrons outside the  $^{56}\text{Ni}$ -core in the

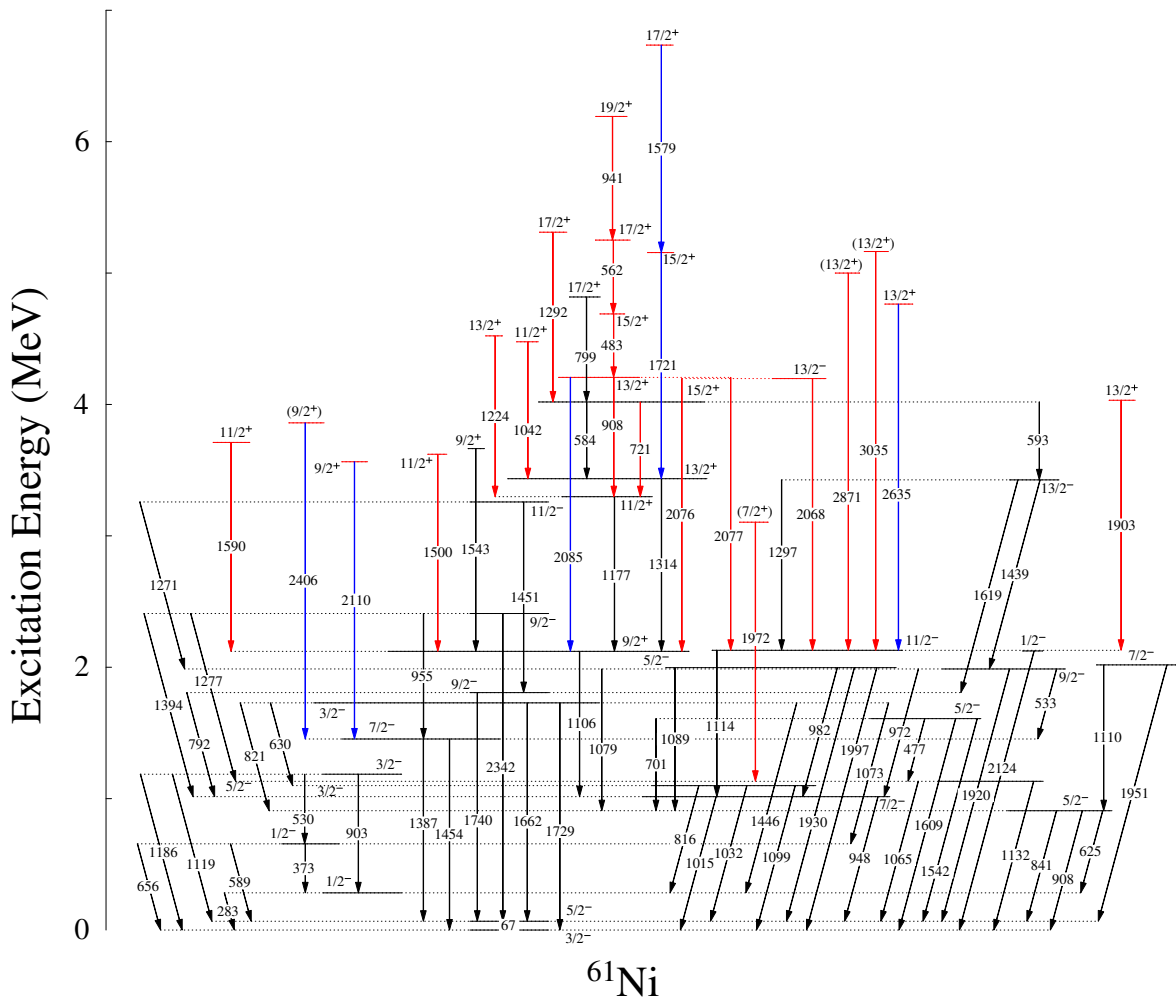


FIG. 4: (Color online) Level scheme of the  $^{61}\text{Ni}$  nucleus from the present work. The new  $\gamma$ -ray transitions identified from the current study are marked in red. The transitions labelled in blue were observed in the previous studies but were either not placed in the level scheme or had different placement with respect to the energy and/or  $J^\pi$  values of the de-exciting states.

$^{61}\text{Ni}$  nucleus were allowed to occupy all the orbitals in the model space without any truncation. Two different interactions, JJ44BPN [16] and JUN45 [17], were used to compute the levels and the results are compared with the measurements in Fig. 7. It follows that the calculated energies, in general, are in reasonable overlap with the experimental ones primarily indicating the shell model configurations underlying the observed states. As far as the negative parity levels are concerned, the JJ44BPN interaction produces comparatively better agreement (of the calculated energies) with the experimental level energies, particularly at low spins (except for the second  $3/2^-$  state that is substantially underpredicted by the JJ44BPN Hamiltonian). At higher spins, the two interactions produce almost similar results. However, for the  $11/2^-$  states, the yrast one better reproduced by the JUN45 interaction vis a vis the deviation of  $\sim 400$  keV in the JJ44BPN calculation. The first non-yrast  $11/2^-$  level, to the contrary, is satisfactorily ( $\sim 150$  keV) represented by the JJ44BPN interaction while the

JUN45 result differs by  $\sim 400$  keV from the experimental energy. In case of the low spin positive parity states, the calculated energies from the two interactions are in agreement with one another and with the experimental ones. However for higher spin positive parity levels, particularly in the range of  $15/2^+$  and beyond, the calculated energies from the JJ44BPN interaction are in better overlap with the experimental results and those using the JUN45 interaction, deviant. The  $13/2^+$  states are exceptions in the aforementioned trend with the energies calculated using JUN45 exhibiting more compliance against those from JJ44BPN. The highest  $17/2^+$  states, however, is grossly underpredicted by either interactions, as illustrated in Fig. 7. These may be issues particular to the interactions and warrant further theoretical investigations. In fact the aforementioned deviations between the theoretical results and the experimental ones can actually be indicative of the required refinements in the model for better compliance with the data.

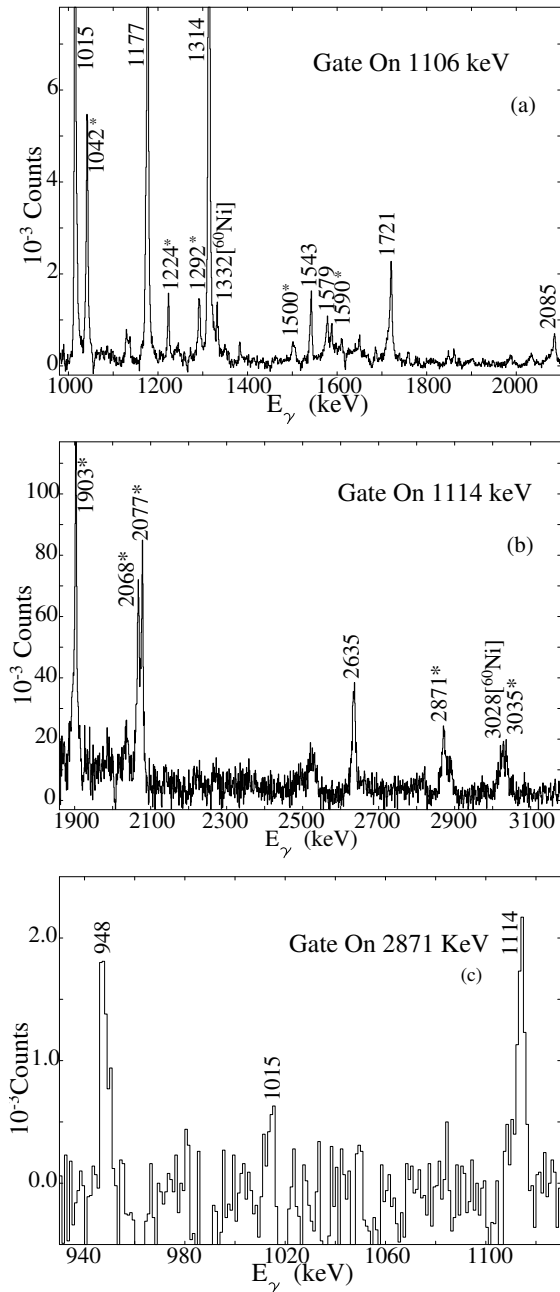


FIG. 5: Representative spectra with gate on  $\gamma$ -ray transitions of  $^{61}\text{Ni}$ , generated from  $\gamma$ - $\gamma$  coincidence matrix. The new transitions, first observed in the present study, are labelled with \*.

The dominant particle configurations constituting the wave functions of the levels are represented in Table II, primarily for the yrast and the first non-yrast level corresponding to each spin. It follows that the positive parity states, observed at higher excitation energies, stem out from one neutron occupation of the  $1g_{9/2}$  orbital. It is interesting to note the possibility of observing the parity changing (E1) transitions associated with such

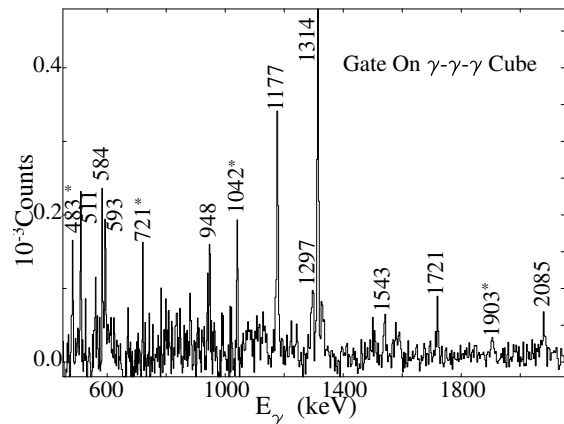


FIG. 6: Sum spectrum with  $\gamma$ - $\gamma$  gate on 948-, 1106-, and 1114-keV transitions in  $^{61}\text{Ni}$ , constructed from the  $\gamma$ - $\gamma$ - $\gamma$  cube. The new transitions, first observed in the present study, are labelled with \*.

excitations into the  $1g_{9/2}$  orbital. Indeed, the transitions 1106-keV ( $9/2^+ \rightarrow 7/2^-$ ), 1903-keV ( $13/2^+ \rightarrow 11/2^-$ ) and 2635-keV ( $13/2^+ \rightarrow 11/2^-$ ) have been identified to be of pure or predominantly E1 character from the present measurements. As far as the negative parity states at higher energies are concerned, they correspond to the excitation of neutrons from  $2p_{3/2}$  orbital to  $1f_{5/2}$  and, still higher,  $2p_{1/2}$  orbitals. Such particle configurations have been obtained from both the interactions used in the present calculations, as recorded in Table II.

TABLE I: Details of energy levels and  $\gamma$ -ray transitions of the  $^{61}\text{Ni}$  nucleus observed in the present work. The uncertainty on the  $\gamma$ -ray energy ( $E_\gamma$ ) has been extracted from fitting of the corresponding transition peak in the spectrum. The uncertainty on the level energy ( $E_i$ ) has been determined by adding the uncertainties on the energies of individual  $\gamma$ -ray transitions, cascading out of the state, in quadrature. If there are more than one  $\gamma$ -ray transition branching out of a level, the one with the highest branching ratio has been considered for evaluating the uncertainty on the level energy.  $E_i^{NND C}$  represents the level energies and the corresponding uncertainties from a least-squares fit to all  $\gamma$ -rays in the level scheme, as carried out by the Nuclear Data Review Group at NNDC [18]. The superscripts in the DCO ratios ( $R_{DCO}$ ) represent the multipolarity of the gating transition,  $D$  for dipole and  $Q$  for quadrupole. The superscript  $N$  represents adoption from NNDC database [19].

$E_i(\text{keV})$	$E_i^{NND C}(\text{keV})$	$E_\gamma(\text{keV})$	$I_\gamma$	$J_i^\pi$	$J_f^\pi$	$R_{DCO}$	$R_{ADO}$	$\Delta_{pol}$	P	Multipolarity
66.7±0.3	67.03±0.14	66.7±0.3	194.3±4.0	5/2 <sup>-</sup>	3/2 <sup>-</sup>		0.71±0.03			M1+E2
283.4±0.3	283.15±0.18	283.4±0.3	4.9±0.3	1/2 <sup>-</sup>	3/2 <sup>-</sup>		0.93±0.13			[E2] <sup>N</sup>
656.0±0.5	656.23±0.19	373.1±0.1	1.0±0.1	1/2 <sup>-</sup>	1/2 <sup>-</sup>		0.80±0.08			M1
		589.0±0.5			5/2 <sup>-</sup>					[E2] <sup>N</sup>
		656.0±0.5			3/2 <sup>-</sup>					(M1+E2) <sup>N</sup>
907.7±0.2	907.73±0.14	625.0±0.5	1.0±0.2	5/2 <sup>-</sup>	1/2 <sup>-</sup>					(E2) <sup>N</sup>
		840.6±0.4	3.9±0.4		5/2 <sup>-</sup>		0.98±0.08			M1+E2
		907.7±0.2	21.8±2.9		3/2 <sup>-</sup>		0.77±0.03	-0.03 ±0.02	-0.41±0.42	M1+E2
1014.6± 0.4	1014.95±0.14	947.9±0.2	151.0±3.8	7/2 <sup>-</sup>	5/2 <sup>-</sup>	0.76±0.05 <sup>Q</sup>	0.98±0.09	-0.01 ±0.01	-0.17±0.25	M1+E2
		1015.1±0.2	50.2±1.4		3/2 <sup>-</sup>	1.02±0.02 <sup>Q</sup>	1.19±0.04			E2
1098.8±0.6	1099.31±0.19	816.1±0.5	2.3±0.2	3/2 <sup>-</sup>	1/2 <sup>-</sup>		0.88±0.05			M1+E2
		1032.4±0.5			5/2 <sup>-</sup>					
		1098.8±0.6			3/2 <sup>-</sup>		0.84±0.07	-0.05 ±0.03	-1.00±1.14	M1+E2
1132.4±0.5	1132.35±0.21	1065.4±0.5		5/2 <sup>-</sup>	5/2 <sup>-</sup>					M1+E2 <sup>N</sup>
		1132.4±0.5			3/2 <sup>-</sup>					M1+E2 <sup>N</sup>
1186.0±0.5	1186.2±0.3	529.6±0.5		3/2 <sup>-</sup>	1/2 <sup>-</sup>					(M1+E2) <sup>N</sup>
		903.2±0.5			1/2 <sup>-</sup>					
		1119.4±0.5			5/2 <sup>-</sup>					
		1186.0±0.5			3/2 <sup>-</sup>					M1+E2 <sup>N</sup>
1454.4±0.5	1454.23±0.18	1386.9±0.2	2.9±0.4	7/2 <sup>-</sup>	5/2 <sup>-</sup>		1.08±0.09			M1+E2
		1454.4±0.5	3.1±0.7		3/2 <sup>-</sup>	0.96±0.07 <sup>Q</sup>	1.19±0.05	0.01 ±0.04	0.28±1.54	E2
1609.0±0.5	1609.2±0.3	477.4±0.5		5/2 <sup>-</sup>	5/2 <sup>-</sup>					
		701.3±0.5	1.0±0.2		5/2 <sup>-</sup>					
		1541.8±0.5	5.6±0.7		5/2 <sup>-</sup>					M1+E2 <sup>N</sup>
		1609.0±0.5			3/2 <sup>-</sup>					M1+E2 <sup>N</sup>
1729.0±1.0	1728.87±0.20	629.5±0.1		3/2 <sup>-</sup>	3/2 <sup>-</sup>		0.63±0.07			M1+E2
		821.3 ±0.5			5/2 <sup>-</sup>					
		1073.4±0.6			1/2 <sup>-</sup>					
		1446.4±0.5			1/2 <sup>-</sup>					
		1662.0±1.0			5/2 <sup>-</sup>					
		1729.0±1.0			3/2 <sup>-</sup>					
1807.1±0.6	1807.31±0.21	792.4±0.3	10.2±0.6	9/2 <sup>-</sup>	7/2 <sup>-</sup>		1.02±0.09			M1+E2
		1740.4±0.5	16.7±0.8		5/2 <sup>-</sup>	1.05±0.05 <sup>Q</sup>	1.22±0.07	0.07 ±0.04	5.62±15.80	E2
1987.0±0.6	1986.93±0.15	532.5±0.3	2.3±0.4	9/2 <sup>-</sup>	7/2 <sup>-</sup>	0.70±0.03 <sup>Q</sup>	0.86±0.07	-0.04 ±0.03	-0.32±0.33	M1+E2
		972.0±0.4	6.0±0.5		7/2 <sup>-</sup>		0.69±0.07			M1+E2
		1079.2±0.1	19.8±2.7		5/2 <sup>-</sup>	1.05±0.04 <sup>Q</sup>	1.17±0.04	0.02 ±0.02	0.40 ±0.58	E2
		1920.3±0.5	13.2±0.6		5/2 <sup>-</sup>	1.03±0.04 <sup>Q</sup>	1.16±0.04	0.02 ±0.02	2.43±12.62	E2
1997.0±1.0	1997.2±0.4	982.4±0.5		5/2 <sup>-</sup>	7/2 <sup>-</sup>					
		1089.4±0.5	1.1±0.2		5/2 <sup>-</sup>					
		1930±1.0	1.0±0.2		5/2 <sup>-</sup>					
		1997±1.0			3/2 <sup>-</sup>					M1+E2 <sup>N</sup>
2017.7±1.0	2017.8±0.5	1110.0±0.5		7/2 <sup>-</sup>	5/2 <sup>-</sup>					
		1951±1.0	2.1±0.3		5/2 <sup>-</sup>					M1(+E2) <sup>N</sup>
2120.6±0.5	2120.88±0.22	1106.0±0.2	100	9/2 <sup>+</sup>	7/2 <sup>-</sup>	0.65±0.01 <sup>Q</sup>	0.82±0.03	0.02±0.02	0.40±0.49	E1
2124.0±1.0	2124.0±1.0	2124.0±1.0		1/2 <sup>-N</sup>	3/2 <sup>-</sup>					
2128.1±0.4	2128.50±0.16	1113.5±0.1	83.6±4.5	11/2 <sup>-</sup>	7/2 <sup>-</sup>	0.99±0.02 <sup>Q</sup>	1.27±0.08	0.03±0.01	0.70±0.84	E2
2409.0±0.4	2409.21±0.21	954.6±0.3	2.0±0.5	9/2 <sup>-</sup>	7/2 <sup>-</sup>					M1+E2 <sup>N</sup>
		1277±1.0			5/2 <sup>-</sup>					E2 <sup>N</sup>
		1394.4±0.2	1.4±0.3		7/2 <sup>-</sup>		0.90±0.09			M1+E2
		2342.0±1.0	2.4±0.3		5/2 <sup>-</sup>					E2 <sup>N</sup>

Continued in next page

TABLE I – continued from previous page

$E_i(keV)$	$E_i^{NNDC}(keV)$	$E_\gamma(keV)$	$I_\gamma$	$J_i^\pi$	$J_f^\pi$	$R_{DCO}$	$R_{ADO}$	$\Delta_{pol}$	P	Multipolarity
3104.7±0.7	3104.7±0.6	1972.3±0.5		(7/2 <sup>+</sup> )	5/2 <sup>-</sup>					
3257.9±0.6	3257.84±0.21	1270.9±0.3	1.2±0.3	11/2 <sup>-</sup>	9/2 <sup>-</sup>					M1+E2 <sup>N</sup>
		1450.5±0.2	2.6±0.3		9/2 <sup>-</sup>	0.73±0.04 <sup>Q</sup>	0.96±0.07	-0.02±0.04	-0.64±1.83	M1+E2
3297.4±0.5	3297.7±0.3	1176.8±0.2	23.6±1.0	11/2 <sup>+</sup>	9/2 <sup>+</sup>		1.04±0.04			M1+E2
3425.7±0.6	3425.63±0.18	1297.0±0.2	9.5±0.5	13/2 <sup>-</sup>	11/2 <sup>-</sup>		0.77±0.03			M1+E2
		1438.7±0.2	13.4±0.7		9/2 <sup>-</sup>	0.96±0.02 <sup>Q</sup>	1.34±0.07	0.029±0.018	1.12±1.73	E2
		1618.5±0.4	5.3±0.4		9/2 <sup>-</sup>	0.95±0.06 <sup>Q</sup>	1.18±0.07	0.02 ±0.03	1.11±2.78	E2
3434.6±0.5	3434.89±0.23	1314.0±0.1	45.4±1.6	13/2 <sup>+</sup>	9/2 <sup>+</sup>		1.27±0.05	0.02 ±0.02	0.53±0.87	E2
3564.7±1.0	3564.6±1.1	2110.3±1.0	1.1±0.3	9/2 <sup>+</sup>	7/2 <sup>-</sup>		0.99±0.08			E1+M2
3621.0±0.6	3621.3±0.5	1500.4±0.4	2.6±0.3	11/2 <sup>+</sup>	9/2 <sup>+</sup>		0.98±0.08			M1+E2
3663.1±0.7	3663.4±0.6	1542.5±0.5	4.0±0.3	9/2 <sup>+</sup>	9/2 <sup>+</sup>	1.58±0.09 <sup>D</sup>	0.87±0.07	-0.04±0.05	-1.67±3.62	M1+E2
3710.1±0.5	3710.4±0.3	1589.5±0.2	3.5±0.4	11/2 <sup>+</sup>	9/2 <sup>+</sup>		0.68±0.05			M1+E2
3860.3±1.0	3860.2±1.1	2405.9±1.0		(9/2 <sup>+</sup> )	7/2 <sup>-</sup>					
4018.3±0.6	4018.28±0.24	583.5±0.3	12.7±0.7	15/2 <sup>+</sup>	13/2 <sup>+</sup>		0.99±0.05			M1+E2
		592.6±0.2	4.8±0.3		13/2 <sup>-</sup>	0.68±0.03 <sup>Q</sup>	0.84±0.03			E1
		720.5±0.6	6.1±0.6		11/2 <sup>+</sup>		1.31±0.06	0.04±0.04	0.46±0.51	E2
4031.5±1.1	4031.9±0.3	1903.4±1.0	3.9±0.3	13/2 <sup>+</sup>	11/2 <sup>-</sup>		0.94±0.07			E1+M2
4196.6±1.0	4196.3±0.5	2067.6±1.5	3.7±0.6	13/2 <sup>-</sup>	11/2 <sup>-</sup>		0.62±0.10			M1+E2
		2076.0±1.0	2.1±0.4		9/2 <sup>+</sup>					
4205.9±1.6	4206.1±0.5	908.4±0.6	4.6±0.5	13/2 <sup>+</sup>	11/2 <sup>+</sup>		0.76±0.07			M1+E2
		2077.4±1.0	4.1±0.4		11/2 <sup>-</sup>	0.77±0.05 <sup>Q</sup>	0.84±0.08			E1+M2
		2085.3±1.5	5.5±0.4		9/2 <sup>+</sup>	1.50±0.10 <sup>D</sup>	1.28±0.06			E2
4476.4±0.5	4476.7±0.3	1041.8±0.2	11.9±0.5	11/2 <sup>+</sup>	13/2 <sup>+</sup>	1.07±0.10 <sup>D</sup>	0.98±0.04	-0.05±0.03	-1.00±1.00	M1+E2
4520.9±0.5	4521.2±0.3	1223.5±0.1	5.8±0.5	13/2 <sup>+</sup>	11/2 <sup>+</sup>	1.09±0.07 <sup>D</sup>	1.02±0.06	-0.03±0.05	-0.79±1.54	M1+E2
4688.4±1.0	4688.7±0.9	482.6±0.7	11.0±0.5	15/2 <sup>+</sup>	13/2 <sup>+</sup>	1.00±0.05 <sup>D</sup>	0.80±0.09	-0.03±0.05	-0.28±0.40	M1
4763.2±1.8	4763.7±0.4	2635.1±1.8	2.6±0.3	13/2 <sup>+</sup>	11/2 <sup>-</sup>		0.93±0.06			E1+M2
4817.0±0.8	4817.0±0.6	798.7±0.5	5.2±0.4	17/2 <sup>+</sup>	15/2 <sup>+</sup>		0.71±0.07	-0.01±0.03	-0.07±0.39	M1+E2
4998.6±2.1	4999.1±1.1	2870.5±2.0	2.1±0.3	(13/2 <sup>+</sup> )	11/2 <sup>-</sup>					
5155.1±0.7	5155.4±0.6	1720.5±0.5	9.5±0.6	15/2 <sup>+</sup>	13/2 <sup>+</sup>		0.96±0.05	-0.03±0.04	-2.14±6.21	M1+E2
5163.5±2.1	5164.0±1.1	3035.4±2.0	2.6±0.3	(13/2 <sup>+</sup> )	11/2 <sup>-</sup>					
5249.9±1.0	5250.3±1.0	561.5±0.5	9.6±0.6	17/2 <sup>+</sup>	15/2 <sup>+</sup>		0.88±0.07			M1+E2
5309.8±0.7	5309.8±0.4	1291.5±0.3	8.5±0.5	17/2 <sup>+</sup>	15/2 <sup>+</sup>		1.00±0.06	-0.07±0.05	-2.21±3.01	M1+E2
6190.4±1.0	6190.8±1.1	940.5±0.5	6.1±0.4	19/2 <sup>+</sup>	17/2 <sup>+</sup>		0.82±0.06			M1
6733.7±0.8	6734.0±0.7	1578.6±0.4	6.2±0.5	17/2 <sup>+</sup>	15/2 <sup>+</sup>	1.01±0.06 <sup>D</sup>	0.95±0.09	-0.01 ±0.05	-0.53±2.81	M1+E2

Higher excitations that can be envisaged in <sup>61</sup>Ni include additional occupancy of 1g<sub>9/2</sub> orbital and breaking of the doubly-magic <sup>56</sup>Ni-core. Such states have not been

observed in the present study and, presumably, requires higher angular momentum input from the projectile used in the fusion-evaporation reaction.

TABLE II: Representative and dominant partitions of wave functions of the positive and negative parity states in <sup>61</sup>Ni calculated using JJ44BPN and JUN45 interactions.

Level Energy			JJ44BPN wave functions			JUN45 wave functions	
EXPT	JJ44BPN	JUN45	$J^\pi$	Probability	Neutron	Probability	Neutron
POSITIVE PARITY							
2121	2123	1937	9/2 <sup>+</sup>	49.50	$f_{5/2}^2 p_{3/2}^2 p_{1/2}^0 g_{9/2}^1$	50.75	$f_{5/2}^2 p_{3/2}^2 p_{1/2}^0 g_{9/2}^1$
3104	2909	3008	(7/2 <sup>+</sup> )	56.97	$f_{5/2}^2 p_{3/2}^2 p_{1/2}^0 g_{9/2}^1$	54.86	$f_{5/2}^2 p_{3/2}^2 p_{1/2}^0 g_{9/2}^1$
3298	3437	3011	11/2 <sup>+</sup>	36.23	$f_{5/2}^1 p_{3/2}^3 p_{1/2}^0 g_{9/2}^1$	61.67	$f_{5/2}^1 p_{3/2}^3 p_{1/2}^0 g_{9/2}^1$
3435	3767	3333	13/2 <sup>+</sup>	29.37	$f_{5/2}^1 p_{3/2}^2 p_{1/2}^0 g_{9/2}^1$	36.93	$f_{5/2}^1 p_{3/2}^3 p_{1/2}^0 g_{9/2}^1$

Continued in next page

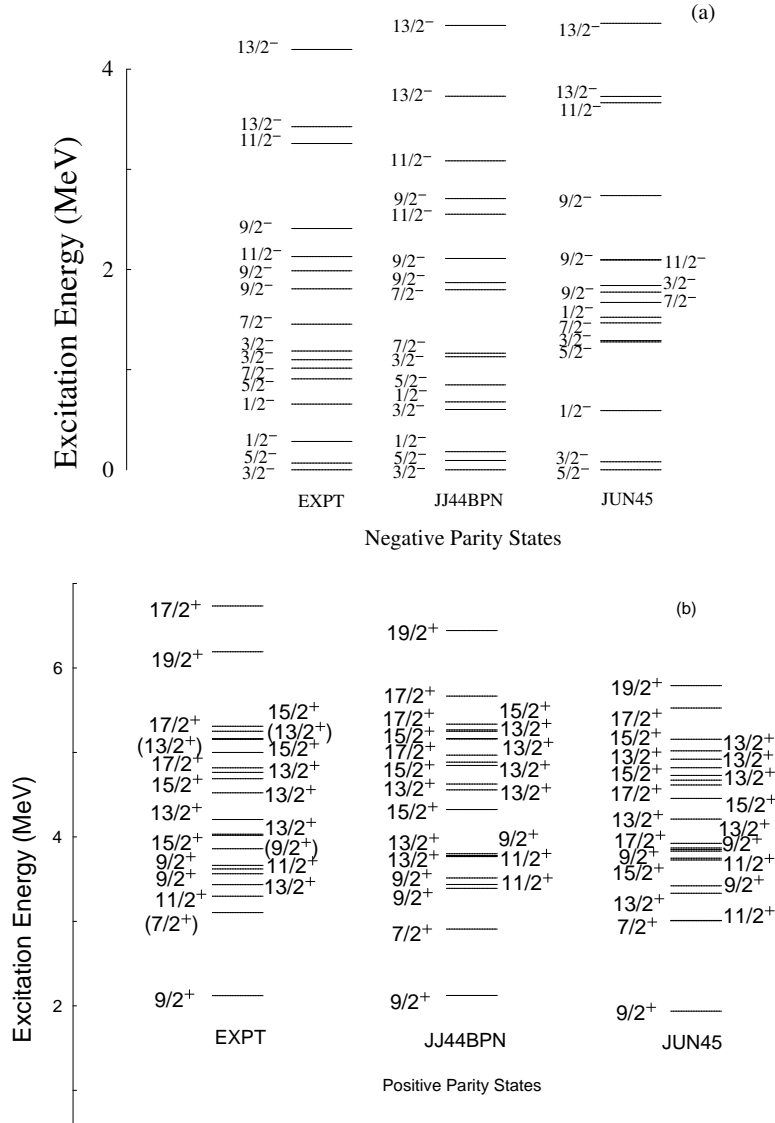


FIG. 7: Comparison of experimental level energies in  $^{61}\text{Ni}$  with those from large basis shell model calculations using JJ44BPN and JUN45 interactions for (a) negative parity states and (b) positive parity states.

TABLEII – continued from previous page

Level Energy		JJ44BPN wave functions			JUN45 wave functions		
EXPT	JJ44BPN	JUN45	$J^\pi$	Probability	Neutron	Probability	Neutron
3564	3391	3421	$9/2^+$	46.31	$f_{5/2}^2 p_{3/2}^2 p_{1/2}^0 g_{9/2}^1$	60.54	$f_{5/2}^2 p_{3/2}^2 p_{1/2}^0 g_{9/2}^1$
3621	3774	3748	$11/2^+$	32.00	$f_{5/2}^2 p_{3/2}^2 p_{1/2}^0 g_{9/2}^1$	55.22	$f_{5/2}^2 p_{3/2}^2 p_{1/2}^0 g_{9/2}^1$
3663	3514	3832	$9/2^+$	46.42	$f_{5/2}^3 p_{3/2}^1 p_{1/2}^0 g_{9/2}^1$	37.16	$f_{5/2}^1 p_{3/2}^3 p_{1/2}^0 g_{9/2}^1$
3860	3801	3869	$(9/2^+)$	23.45	$f_{5/2}^2 p_{3/2}^2 p_{1/2}^0 g_{9/2}^1$	37.36	$f_{5/2}^2 p_{3/2}^2 p_{1/2}^0 g_{9/2}^1$
4019	4324	3727	$15/2^+$	52.59	$f_{5/2}^1 p_{3/2}^3 p_{1/2}^0 g_{9/2}^1$	51.65	$f_{5/2}^1 p_{3/2}^3 p_{1/2}^0 g_{9/2}^1$
4032	4203	3924	$13/2^+$	31.16	$f_{5/2}^3 p_{3/2}^1 p_{1/2}^0 g_{9/2}^1$	38.75	$f_{5/2}^2 p_{3/2}^2 p_{1/2}^0 g_{9/2}^1$

Continued in next page

TABLEII – continued from previous page

Level Energy			JJ44BPN wave functions				JUN45 wave functions	
EXPT	JJ44BPN	JUN45	$J^\pi$	Probability	Neutron	Probability	Neutron	
4206	4557	4211	$13/2^+$	33.02	$f_{5/2}^3 p_{3/2}^1 p_{1/2}^0 g_{9/2}^1$	30.71	$f_{5/2}^2 p_{3/2}^2 p_{1/2}^0 g_{9/2}^1$	
4521	4626	4728	$13/2^+$	25.36	$f_{5/2}^2 p_{3/2}^2 p_{1/2}^0 g_{9/2}^1$	32.77	$f_{5/2}^2 p_{3/2}^2 p_{1/2}^0 g_{9/2}^1$	
4689	4885	4456	$15/2^+$	39.37	$f_{5/2}^3 p_{3/2}^1 p_{1/2}^0 g_{9/2}^1$	44.01	$f_{5/2}^2 p_{3/2}^2 p_{1/2}^0 g_{9/2}^1$	
4763	4846	4819	$13/2^+$	30.83	$f_{5/2}^1 p_{3/2}^3 p_{1/2}^0 g_{9/2}^1$	43.07	$f_{5/2}^2 p_{3/2}^2 p_{1/2}^0 g_{9/2}^1$	
4818	4968	3850	$17/2^+$	33.63	$f_{5/2}^2 p_{3/2}^2 p_{1/2}^0 g_{9/2}^1$	42.18	$f_{5/2}^1 p_{3/2}^3 p_{1/2}^0 g_{9/2}^1$	
4999	5159	4920	$(13/2^+)$	43.32	$f_{5/2}^3 p_{3/2}^1 p_{1/2}^0 g_{9/2}^1$	38.80	$f_{5/2}^2 p_{3/2}^2 p_{1/2}^0 g_{9/2}^1$	
5155	5165	4672	$15/2^+$	43.49	$f_{5/2}^3 p_{3/2}^1 p_{1/2}^0 g_{9/2}^1$	46.82	$f_{5/2}^2 p_{3/2}^2 p_{1/2}^0 g_{9/2}^1$	
5164	5267	5019	$(13/2^+)$	28.30	$f_{5/2}^2 p_{3/2}^2 p_{1/2}^0 g_{9/2}^1$	31.75	$f_{5/2}^2 p_{3/2}^2 p_{1/2}^0 g_{9/2}^1$	
5251	5251	4615	$17/2^+$	41.86	$f_{5/2}^2 p_{3/2}^2 p_{1/2}^0 g_{9/2}^1$	46.67	$f_{5/2}^2 p_{3/2}^2 p_{1/2}^0 g_{9/2}^1$	
5310	5335	5156	$15/2^+$	34.01	$f_{5/2}^3 p_{3/2}^1 p_{1/2}^0 g_{9/2}^1$	38.37	$f_{5/2}^2 p_{3/2}^2 p_{1/2}^0 g_{9/2}^1$	
6192	6443	5791	$19/2^+$	51.89	$f_{5/2}^3 p_{3/2}^1 p_{1/2}^0 g_{9/2}^1$	61.66	$f_{5/2}^2 p_{3/2}^2 p_{1/2}^0 g_{9/2}^1$	
6734	5667	5526	$17/2^+$	37.09	$f_{5/2}^3 p_{3/2}^1 p_{1/2}^0 g_{9/2}^1$	82.35	$f_{5/2}^2 p_{3/2}^2 p_{1/2}^0 g_{9/2}^1$	
NEGATIVE PARITY								
0	0	80	$3/2^-$	46.05	$f_{5/2}^2 p_{3/2}^3 p_{1/2}^0 g_{9/2}^0$	60.52	$f_{5/2}^2 p_{3/2}^3 p_{1/2}^0 g_{9/2}^0$	
67	93	0	$5/2^-$	36.77	$f_{5/2}^3 p_{3/2}^2 p_{1/2}^0 g_{9/2}^0$	46.60	$f_{5/2}^1 p_{3/2}^4 p_{1/2}^0 g_{9/2}^0$	
283	181	591	$1/2^-$	38.26	$f_{5/2}^0 p_{3/2}^4 p_{1/2}^0 g_{9/2}^0$	33.51	$f_{5/2}^0 p_{3/2}^4 p_{1/2}^0 g_{9/2}^0$	
656	678	1523	$1/2^-$	40.60	$f_{5/2}^2 p_{3/2}^2 p_{1/2}^0 g_{9/2}^0$	20.94	$f_{5/2}^2 p_{3/2}^2 p_{1/2}^0 g_{9/2}^0$	
908	848	1277	$5/2^-$	21.93	$f_{5/2}^1 p_{3/2}^3 p_{1/2}^0 g_{9/2}^0$	33.79	$f_{5/2}^3 p_{3/2}^2 p_{1/2}^0 g_{9/2}^0$	
1015	1164	1467	$7/2^-$	33.85	$f_{5/2}^2 p_{3/2}^3 p_{1/2}^0 g_{9/2}^0$	29.27	$f_{5/2}^3 p_{3/2}^2 p_{1/2}^0 g_{9/2}^0$	
1099	602	1290	$3/2^-$	46.01	$f_{5/2}^3 p_{3/2}^2 p_{1/2}^0 g_{9/2}^0$	32.91	$f_{5/2}^3 p_{3/2}^2 p_{1/2}^0 g_{9/2}^0$	
1186	1129	1840	$3/2^-$	31.33	$f_{5/2}^2 p_{3/2}^2 p_{1/2}^0 g_{9/2}^0$	23.19	$f_{5/2}^2 p_{3/2}^3 p_{1/2}^0 g_{9/2}^0$	
1454	1798	1671	$7/2^-$	27.50	$f_{5/2}^2 p_{3/2}^2 p_{1/2}^0 g_{9/2}^0$	58.92	$f_{5/2}^2 p_{3/2}^3 p_{1/2}^0 g_{9/2}^0$	
1807	1869	1774	$9/2^-$	40.01	$f_{5/2}^3 p_{3/2}^2 p_{1/2}^0 g_{9/2}^0$	57.80	$f_{5/2}^2 p_{3/2}^3 p_{1/2}^0 g_{9/2}^0$	
1987	2110	2097	$9/2^-$	56.08	$f_{5/2}^3 p_{3/2}^2 p_{1/2}^0 g_{9/2}^0$	46.58	$f_{5/2}^3 p_{3/2}^2 p_{1/2}^0 g_{9/2}^0$	
2129	2552	2096	$11/2^-$	68.84	$f_{5/2}^2 p_{3/2}^3 p_{1/2}^0 g_{9/2}^0$	79.32	$f_{5/2}^2 p_{3/2}^3 p_{1/2}^0 g_{9/2}^0$	
2409	2708	2738	$9/2^-$	24.43	$f_{5/2}^2 p_{3/2}^2 p_{1/2}^0 g_{9/2}^0$	53.10	$f_{5/2}^3 p_{3/2}^2 p_{1/2}^0 g_{9/2}^0$	
3258	3085	3665	$11/2^-$	56.64	$f_{5/2}^4 p_{3/2}^1 p_{1/2}^0 g_{9/2}^0$	43.83	$f_{5/2}^2 p_{3/2}^2 p_{1/2}^0 g_{9/2}^0$	
3426	3730	3728	$13/2^-$	87.03	$f_{5/2}^3 p_{3/2}^2 p_{1/2}^0 g_{9/2}^0$	88.80	$f_{5/2}^3 p_{3/2}^2 p_{1/2}^0 g_{9/2}^0$	

Continued in next page

TABLE II – continued from previous page

Level Energy		JJ44BPN wave functions			JUN45 wave functions		
EXPT	JJ44BPN	JUN45	$J^\pi$	Probability	Neutron	Probability	Neutron
4197	4437	4458	$13/2^-$	66.05	$f_{5/2}^2 p_{3/2}^2 p_{1/2}^1 g_{9/2}^0$	76.35	$f_{5/2}^2 p_{3/2}^2 p_{1/2}^1 g_{9/2}^0$

#### IV. CONCLUSION

Excited states of the  $^{61}\text{Ni}$  nucleus have been studied following their population in heavy-ion induced fusion-evaporation reaction and using an array of Compton suppressed germanium (clover) detectors as the detection system. The level structure of the nucleus has been established upto an excitation energy of  $\sim 7$  MeV and spin  $\sim 10\hbar$ . The multipolarity and electromagnetic nature of the  $\gamma$ -ray transitions have been measured and spin-parity assignments have been made to the observed levels. Large basis shell model calculations have been carried out in the  $fp$  model space with unrestricted occupation of the orbitals and two different interactions. The calculated level energies have been found to be in reasonable overlap with the experimental ones. The wave functions of the negative parity states have been calculated to be constituted with occupation of  $fp$  orbitals and that of the positive parity states, observed at higher excitation energies, corresponds to excitation of a single neutron to the  $g_{9/2}$  orbital. The present endeavor thus identifies the one-particle excitations into the  $g_{9/2}$  orbital in the evolution of particle occupancy, with increasing energy and spin, for the  $^{61}\text{Ni}$  nucleus. Multiparticle excitations into the  $g_{9/2}$  orbital and core-broken configurations have not been observed in this measurement and will probably require higher angular momentum input in the reaction

used for producing the nucleus of interest. However, the observed deviations between the calculated level energies and the measured ones may provide an impetus for refinements in the corresponding shell model interactions that would result in an improved overlap of the theoretical results with the experimental data.

#### Acknowledgment

The authors wish to thank the staff of the Pelletron LINAC Facility at TIFR, Mumbai, for their help and support during the experiment. Our deepest gratitude to Smt. Deepa Teksingh Pujara of the Target Laboratory at TIFR for her guidance, help and active contribution during the target fabrication exercise. Help and support received from Mr. Kausik Basu (UGC-DAE CSR, KC), Mr. B. S. Naidu, Mr. S. Jadhav and Mr. R. Donthi (TIFR), during the experiment, is appreciated. We are grateful to the Nuclear Data Review Group at NNDC, Brookhaven National Laboratory, for the data consistency check on the manuscript and the least-squares fit calculation of the level energies. This work is partially supported by the Department of Science and Technology, Government of India (No. IR/S2/PF-03/2003-II) and the US National Science Foundation (Grant No. PHY1762495).

- 
- [1] S. Samanta, S. Das, R. Bhattacharjee, S. Chatterjee, S. S. Ghugre, A. K. Sinha, U. Garg, Neelam, N. Kumar, P. Jones, et al., Phys. Rev. C **97**, 014319 (2018).
  - [2] D. A. Torres, F. Cristancho, L. L. Andersson, E. K. Johansson, D. Rudolph, C. Fahlander, J. Ekman, R. du Rietz, C. Andreoiu, M. P. Carpenter, et al., Phys. Rev. C **78**, 054318 (2008).
  - [3] R. Wadsworth, G. D. Jones, A. Kogan, P. R. G. Lornie, T. Morrison, . Mustafa, H. G. Price, D. Simister, and P. J. Twin, J. Phys. G **3**, 833 (1977).
  - [4] R. Wadsworth, A. Kogan, P. R. G. Lornie, M. R. Nixon, H. G. Price, and P. J. Twin, J. Phys. G **3**, 35 (1977).
  - [5] E. K. Warburton, J. W. Olness, A. M. Nathan, and A. R. Poletti, Phys. Rev. C **18**, 1637 (1978).
  - [6] R. A. Meyer, A. L. Prindle, W. A. Myers, P. K. Hopke, D. Dieterly, and J. E. Koops, Phys. Rev. C **17**, 1822 (1978).
  - [7] J. E. Koops and P. W. M. Glaudemans, Z. Phys. A **280**, 181 (1977).
  - [8] G. Satyanarayana, N. V. Rao, G. S. S. Krishna, M. V. S. C. Rao, S. B. Reddy, D. L. Sastry, S. N. Chinthalapudi, and V. V. Rao, IL Nuovo Cimento A **99**, 309 (1988).
  - [9] S. Raman, X. Ouyang, M. A. Islam, J. W. Starner, E. T. Jurney, E. Y. Lynn, and G. Martinez-Pinedo, Phys. Rev. C **70**, 044318 (2004).
  - [10] R. Palit, S. Saha, J. Sethi, T. Trivedi, S. Sharma, B. S. Naidu, S. Jadhav, R. Donthi, P. B. Chavan, H. Tan, et al., Nucl. Instr. Meth. Phys. Res. A **680**, 90 (2012).
  - [11] D. C. Radford, Nucl. Instr. Meth. Phys. Res. A **361**, 297 (1995).
  - [12] M. Piiparinen, A. Atac, J. Blomqvist, G. B. Hagemann, B. Herskind, R. Julin, S. Juutinen, A. Lampinen, J. Nyberg, G. Sletten, et al., Nucl. Phys. A **605**, 191 (1996).
  - [13] R. Palit, H. C. Jain, P. K. Joshi, S. Nagaraj, B. V. T. Rao, S. N. Chinthalapudi, and S. S. Ghugre, Pramana **54**, 347 (2000).
  - [14] B. A. Brown and B. Wildenthal, Annu. Rev. Nucl. Part. Sci. **38**, 29 (1988).
  - [15] W. A. Richter, S. Mkhize, and B. A. Brown, Phys. Rev. C **78**, 064302 (2008).
  - [16] A. F. Lisetskiy, B. A. Brown, M. Horoi, and H. Grawe, Phys. Rev. C **70**, 044314 (2004).
  - [17] M. Honma, T. Otsuka, T. Mizusaki, and M. Hjorth-Jensen, Phys. Rev. C **80**, 064323 (2009).

[18] NNDC, Priv. Comm. (2018).

[19] URL [www.nndc.bnl.gov](http://www.nndc.bnl.gov).